Adsorption of unfolded Cu/Zn superoxide dismutase onto hydrophobic surfaces catalyzes its formation of amyloid fibrils

Khan, Ashhar; Weininger, Ulrich; Kjellström, Sven; Deep, Shashank; Akke, Mikael

Published in:
Protein Engineering Design & Selection

DOI:
10.1093/protein/gzz033

2019

Document Version:
Early version, also known as pre-print

Adsorption of Unfolded Cu/Zn Superoxide Dismutase onto Hydrophobic Surfaces Catalyzes Its Formation of Amyloid Fibrils

M. Ashhar I. Khan[1,2], Ulrich Weininger[1], Sven Kjellström[3], Shashank Deep[2], Mikael Akke[1,*]

[1] Biophysical Chemistry, Center for Molecular Protein Science, Department of Chemistry, Lund University, Lund, Sweden

[2] Department of Chemistry, Indian Institute of Technology Delhi, New Delhi, India

[3] Biochemistry and Structural Biology, Center for Molecular Protein Science, Department of Chemistry, Lund University, Lund, Sweden

* Correspondence to: mikael.akke@bpc.lu.se

Running title: Hydrophobic surfaces catalyze fibrillation of unfolded SOD1

Abstract

Intracellular aggregates of superoxide dismutase 1 (SOD1) are associated with amyotrophic lateral sclerosis (ALS). In vivo, aggregation occurs in a complex and dense molecular environment with chemically heterogeneous surfaces. To investigate how SOD1 fibril formation is affected by surfaces, we used an in vitro model system enabling us to vary the molecular features of both SOD1 and the surfaces, as well as the surface area. We compared fibril formation in hydrophilic and hydrophobic sample wells, as a function of denaturant concentration and extraneous hydrophobic surface area. In the presence of hydrophobic surfaces, SOD1 unfolding promotes fibril nucleation. By contrast, in the presence of hydrophilic surfaces, increasing denaturant concentration retards the onset of fibril formation. We conclude that the mechanism of fibril formation depends on the surrounding surfaces, and that the nucleating species might correspond to different conformational states of SOD1 depending on the nature of these surfaces.

Keywords: amyotrophic lateral sclerosis; protein aggregation; protein unfolding; surface adsorption; surface catalyzed nucleation

Introduction

Numerous pathological conditions have been discovered over the years in which protein aggregation is reported to be the primary causing agent. Among them are various neurodegenerative diseases such as Alzheimer's disease, Parkinson disease and amyotrophic lateral sclerosis (ALS) (Dobson, 2003; Luheshi *et al.*, 2008). ALS is an adult-onset fatal neurodegenerative disorder that causes motor neuron degeneration in the cortex, spinal cord and brainstem, causing progressive paralysis and ultimately death (Ajroud-Driss and Siddique, 2015; Morgan and Orrell, 2016). A subset of ALS cases are associated with intracellular aggregates of Cu/Zn superoxide dismutase (SOD1), and more than 160 mutations in SOD1 have been recognized to date in ALS patients (Ajroud-Driss and Siddique, 2015; Morgan and Orrell, 2016). A large body of work on SOD1 aggregation in cells and in vivo has provided fundamental insights into key aspects of this process (Wang *et al.*, 2002, 2006; Karch and Borchelt, 2008; Karch *et al.*, 2009; Roberts *et al.*, 2012; Banci *et al.*, 2013; Luchinat *et al.*, 2014). Mounting evidence suggests that aggregation of wildtype SOD1 also might trigger ALS (Gruzman *et al.*, 2007; Bosco *et al.*, 2010; Forsberg *et al.*, 2010).

In its metal-ion bound state, SOD1 is a very stable homodimeric protein, whose 153-residue subunits fold into a β-barrel composed of eight anti-parallel β strands arranged in a conserved Greek key motif (Tainer *et al.*, 1982; Valentine *et al.*, 2005), see Figure 1. Each subunit coordinates one copper and one zinc atom, and contains a highly conserved intra-molecular disulfide bond (C57-C146) in the reducing environment of the cytosol. Reduction of the disulfide bond and loss of metal ions lead to significant

destabilization of SOD1 and dissociation of the dimer into monomers (Hough *et al.*, 2004; Khare *et al.*, 2004; Rakhit *et al.*, 2004). The resulting monomeric, disulfide reduced and metal-ion free (apo) state is the most immature species of SOD1 expected in the cell and it could conceivably accumulate under various conditions of cell stress. A large number of studies have implicated this species as the precursor of aggregated forms (Hough *et al.*, 2004; Khare *et al.*, 2004; Rakhit *et al.*, 2004; Lang *et al.*, 2012; Khan *et al.*, 2017). In keeping with the general view of amyloid formation (Chiti and Dobson, 2006, 2009) it is believed that a partially or globally unfolded conformation of SOD1 is the starting point for aggregation. Indeed, NMR relaxation experiments have shown that monomeric apo SOD1 transiently samples partially unfolded conformations that form non-native dimers (Teilum *et al.*, 2009; Sekhar *et al.*, 2015), which potentially are the earliest species along the aggregation pathway.

Interactions between amyloidogenic proteins and membrane surfaces play a prominent role in fibril formation and toxicity in vivo (Stefani, 2007; Aisenbrey *et al.*, 2008; Lu *et al.*, 2016). Association of proteins onto a surface can increase the effective concentration and reduce the stability of the native state, thereby nucleating aggregation. In vitro studies have shown that various model surfaces affect amyloid formation kinetics, as well as the size and structure of the resulting aggregates (Zhu *et al.*, 2002; Linse *et al.*, 2007; Morinaga *et al.*, 2010; Pronchik *et al.*, 2010; Moores *et al.*, 2011). Although the aggregation behavior depends on the physicochemical properties of both the protein and the surface, it is generally found that hydrophobic or charged surfaces tend to promote protein adsorption and aggregation (Zhu *et al.*, 2002; Stefani, 2007;

Morinaga *et al.*, 2010; Pronchik *et al.*, 2010; Moores *et al.*, 2011), whereas neutral, hydrophilic (e.g. PEGylated) surfaces diminish these effects (Alcantar *et al.*, 2000; Pronchik *et al.*, 2010).[25, 28]

Because SOD1 is quite resistant to aggregation under near-physiological conditions in vitro, previous studies have resorted to sample agitation as a means to trigger the formation of amyloid fibrils (Chattopadhyay *et al.*, 2008, 2015; Lang *et al.*, 2012). It should be noted that agitated experiments involve hydrophobic surfaces both in the form of increased air-water interface and teflon-coated stirrers. By contrast, we recently demonstrated that monomeric, disulfide reduced, apo SOD1 forms amyloid fibrils under non-denaturing, non-agitated conditions on a time scale of roughly one week (Khan *et al.*, 2017). In our previous study we monitored fibril formation using PEGylated microplates, and found that increasing denaturant concentration delayed the onset of fibril formation. This result is in contrast to those obtained on agitated samples, where increasing denaturant concentration leads to shortened lag times for aggregation (Oztug Durer *et al.*, 2009; Lang *et al.*, 2012).

There are two plausible, non-exclusive explanations for the different responses to denaturants observed for SOD1 in quiescent and agitated experiments. First, the greater hydrophobic surface, contributed by the air-water interface and teflon-coated stirrers, present in agitated samples is expected to favor adsorption of unfolded protein with exposed hydrophobic patches, which increase with increasing denaturant concentration, leading to surface-catalyzed nucleation of fibril formation (Morinaga *et al.*, 2010; Pronchik *et al.*, 2010). By contrast, in the case of non-agitated experiments using

PEGylated sample containers, denaturants apparently destabilize aggregated species, such as oligomers and fibrils, and this effect is more important than the concomitant destabilization of the native monomeric state, leading to a delayed onset of fibril formation (Khan *et al.*, 2017). In the presence of extraneous hydrophobic surfaces the destabilizing effect of denaturants on aggregated species is apparently reduced significantly. Second, agitation causes fibril fragmentation (Xue *et al.*, 2008; Knowles *et al.*, 2009; Morinaga *et al.*, 2010; Abdolvahabi *et al.*, 2017), which might be further augmented by destabilizing effects of the denaturant on the fibril, leading to enhanced fibril formation. Obviously, this effect is mitigated in non-agitated experiments.

Here we describe how SOD1 fibril formation is affected by increasing the hydrophobic surface area present in the sample container. We address the questions whether hydrophobic surfaces alone, without mechanical agitation, is sufficient to catalyze fibril formation of SOD1, and whether addition of denaturants, causing unfolding of the protein, increases or decreases the lag time for fibril formation under these conditions. Furthermore, we follow up on previous work by comparing the fibril formation of SOD1 variants that perturb important structural features, namely the intramolecular disulfide bridge, cysteine residues, and the long, flexible loops IV and VII. We show that fibril nucleation is indeed catalyzed by hydrophobic surfaces also under quiescent conditions. Global unfolding further shortens the lag time in the presence of hydrophobic surfaces in the case of SOD1 variants that perturb the structural features mentioned above, whereas disulfide-linked apo-SOD1 does not form fibrils under the same conditions and a similar time span.

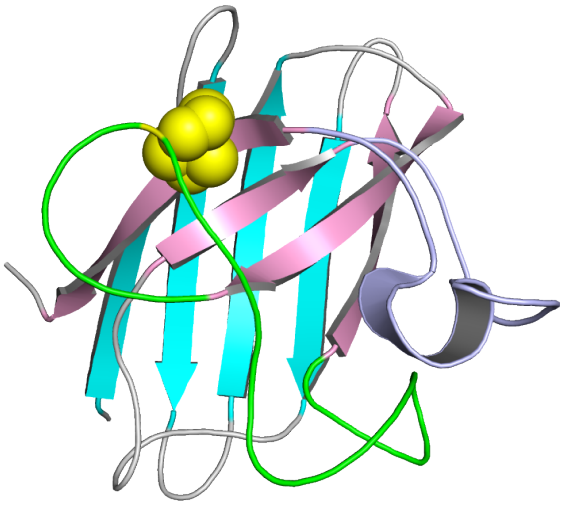

Figure 1. Structure of apo monomeric pwt-SOD1. The two β-sheets are colored cyan (strands 1, 2, 3 and 6) and pink (strands 4, 5, 7 and 8), loop IV is green, loop VII is purple, and other turns and loops are gray. The atoms of the side chains forming the C57–C146 disulfide bond are highlighted as yellow spheres. In $SOD1^{\Delta C}$, C57 and C146 are replaced with serine residues. In $SOD1^{LL}$, loops IV (green) and VII (purple) are replaced with Gly-Ala-Gly tripeptide linkers. The figure was made using the PyMOL molecular graphics system (Schrödinger, LLC) and PDB entry 2xjk (Leinartaitè *et al.*, 2010), which represents the Cu- and Zn-bound state of the monomeric, pseudo-wildtype variant C6A/F50E/G51E/C111A employed in the present study.

Materials and Methods

Materials. All chemicals were of analytical grade and purchased from Sigma-Aldrich (USA). All experiments were performed in 20 mM 3-(N-morpholino)-propanesulfonic

acid (MOPS) buffer at pH 7.0, unless otherwise specified. Tris(2-carboxyethyl)phosphine (TCEP) solution neutralized with NaOH was used as reducing agent. The concentrations of ultrapure urea (Bioxtra) determined by measuring their refractive index.Uncharged plain polystyrene nanoparticles (PS-NP) of 24 nm diameter, with a standard deviation of < 10%, were obtained from Bangs Laboratories Inc. (Fishers, IN, USA) and diluted in the experimental buffer a day before use. The PS-NP size distribution was also independently confirmed in-house using dynamic light scattering (DLS) on Dyno Pro Plate reader, yielding an average hydrodyamic radius of 11.5nm. All solutions were prepared in ultrapure water (<18.2 MΩcm at 25 °C, MilliQ grade). All reagents and buffers were filtered through a 0.22 μm cutoff filter and degassed before use. The pH of all reagents and buffers was maintained at 7.0 unless stated otherwise.

Plasmid design. The plasmids were designed as described (Teilum *et al.*, 2009) and obtained from GenScript USA, Inc. All constructs used herein are based on the well-established pseudo-wild typevariant of SOD1 (pwt-SOD1), which is a quadruple point mutant of human wild-typeSOD1: C6A/F50E/G51E/C111A; the C to A mutations ensure that aberrant disulfide linkages cannot form and the F50E and G51E mutations introduce charged groups at the dimer interface, thereby making the protein monomeric (Bertini *et al.*, 1994; Teilum *et al.*, 2009). The structure of pwt-SOD1 shows no significant deviations from wild-type SOD1 (Hörnberg *et al.*, 2007). We also used a cysteine-free mutant ($SOD1^{\Delta C}$) that includes the C57S and C146S mutations on the background of the pwt-SOD1 template (Khan *et al.*, 2017). Furthermore, for comparison with previous studies (Danielsson *et al.*, 2011) we also included the loop-less variant ($SOD1^{LL}$), in

which both the metal-binding loop (residues 49–81, loop IV) and electrostatic loop (residues 124–139, loop VII) are replaced by Gly-Ala-Gly tripeptide linkers. The removal of loop IV eliminates a number of dimer interface residues, including F50 and Gl51, as well as C57. Since C57 forms part of the native disulfide bridge, C57–Cys146, $SOD1^{LL}$ also includes the C146S mutation, so as to avoid formation of aberrant intermolecular disulfide links. Intact mass determination and sequence composition of all expressed protein constructs were confirmed by MALDI mass spectrometry (see Figure S3, Supporting Information).

Protein expression and purification. pwt-SOD1 and other variantswere expressed in *Escherichia coli* strain BL21 (DE3) pLysS* and purified as described previously (Lindberg *et al.*, 2002; Teilum *et al.*, 2009), except that the heat denaturation step was not included for $SOD1^{\Delta C}$ and $SOD1^{LL}$. All variants were initially purified using size-exclusion gel chromatography, followed by purification on Source 15Q anion-exchange column. Apo SOD1 was prepared by extensive dialysis against 100 mM sodium acetate buffer at pH 3.8 in the presence of 10 mM EDTA followed by thorough dialysis against 20 mM MOPS buffer, pH 7.0.The proteins were concentrated using Vivaspin 2 (3.0 kDa M_w cut-off, PES, Sartorius) centrifugal concentrators before storage.

Fibril assay. To ensure reproducibility, every experiment was started with the isolation of pure monomeric SOD1 using fast protein liquid chromatography (FPLC) employing an analytical size-exclusion column (Superdex 75 10/300 GL) equilibrated with 20 mM MOPS buffer pH 7.0. Only the central portion of the monomer peak (Figure S4, Supporting Information) was collected to minimize any contamination from bacterial

proteins or preexisting aggregates. NMR spectra acquired on freshly prepared monomeric samples verifies that all SOD1 variants are folded (Khan *et al.*, 2017). Thus, all experiments conducted in the absence of denaturants were initiated using folded, monomeric protein. The concentration of the collected protein fraction was estimated by measuring the absorbance at 280 nm on a NanoDrop 2000/2000c spectrophotometer (Thermo Scientific), using an extinction coefficient of 5500 $M^{-1}cm^{-1}$. Samples were prepared with 40 μM thioflavinT (ThT) and 200 μM protein dissolved in 20 mM MOPS buffer pH 7.0. Different sample conditions were screened by adding TCEP and urea in different combinations and concentrations, see SI Tables S1–3 for a complete listing. All samples were prepared in low-binding Eppendorf tubes (Genuine Axygen quality, micro tubes MCT-200-L-C) and kept on ice before distributing them in aliquots onto 96-well half-area plates of two types, either polyethylene glycol-coated black polystyrene (denoted PEG) plates with clear bottom (Corning 3881) or black polystyrene (denoted PS) plates with clear and flat bottom (Costar 3631). Sample aliquots of 100 μl and 150 μl were distributed onto the PEG and PS plates, respectively.

Each sample was run in triplicate, distributed on the plate in a random manner to mitigate the effects of potential temperature variations across the plate during measurement. Plates were sealed with a plastic film (Corning 3095) and placed in either a Fluostar Omega or Polarstar Optima plate reader (BMG Labtech, Offenburg, Germany) and incubated at 37 °C without explicit agitation. ThT fluorescence was monitored every 3 min through the bottom of the plate, with the excitation and emission wavelengths set to 440 nm and 480 nm, respectively.

We used polystyrene nanoparticles to study the dependence of fibril formation on hydrophobic surface area. We estimated the amount of PS nanoparticles required to provide surface area equivalent to that present in a 150 µl well on a PS plate and mixed this amount with 100 µl of protein solution in PEG plate wells. We carried out a gradient experiment using PEG plates with increasing amounts of PS nanoparticles added to the sample wells to yield a total hydrophobic surface area ranging from approximately 1.25–12.5 cm^2. Control experiments were also performed with PS nanoparticles, but without any protein, to check that ThT fluorescence is not affected by nanoparticles in a time-dependent manner; however, scattering by nanoparticles do affect the intensity measured by the detector (see Figure S2).

Transmission electron microscopy. Aggregates were visualized by transmission electron microscopy (TEM). Approximately 8 µl of fresh SOD1 aggregates taken from the 96-well plate were applied on 300-mesh carbon-coated grid with Formvar carbon film (EM Sciences). Samples were allowed to adsorb for 2 minutes. After washing with Milli-Q water, negative staining with 1.5% uranyl acetate (UA) was performed for 30 seconds. Excessive UA solution was removed and the grid was blotted dry. Images were obtained on a Philips CM120 BioTWINCryo equipped with a postcolumn energy filter (Gatan GIF100), operating at an acceleration voltage of 120 kV. The images were recorded digitally with a CCD camera under low electron dose conditions at a magnification of 1:31,000.

Mass spectrometry peptide mass fingerprinting. Peptide mass fingerprinting were carried out on a MALDI-TOF-TOF-MS instrument, Applied Biosystems Proteomics

Analyser 4700 (Applied Biosystems, Framingham, MA). The matrix solution consisted of 5 mg/mlα-cyano-4-cinnamic acid (α-CHCA) dissolved in acetonitrile phosphoric acid (50:0.1 v/v). 10 fmol/µl of des-Arg-Bradykinin, m/z 904.468 and 20 fmol/µl of ACTH 18-39, m/z 2465.199, were added to the matrix solution as internal standards. For the analysis, 0.2 µl of sample was mixed with 0.2 µl matrix solution on the MALDI target plate. For the peptide mass fingerprint analysis, a rapid digestion (60 minutes) using sequence-grade trypsin (Promega) at 1:20 and 1:50 trypsin:protein ratio (w/w) was performed. 50% acetonitrile in 25 mM NH_4HCO_3 was used as the digestion buffer. The peptide mass fingerprint analysis was performed using the reflector mode of the instrument and subsequent analysis of peptides was performed in MS/MS mode. Detailed information about digestion pattern and analysis is given in Supplementary data (Figure S3).

Results and Discussion

Fibril formation in vivo takes place in the context of the complex and dense molecular environment of the living cell, with chemically heterogeneous surfaces presented by soluble proteins, aggregates and membranes. It is expected that the propensity and mechanism of fibril formation depends on the physicochemical properties of both the amyloidogenic protein and its environment. To investigate how fibril formation by SOD1 might be tuned by the nature of the surrounding surfaces, we used a well-defined in vitro model system that allowed us to vary the molecular features of both the protein and the surfaces, as well as the surface area.

First, we studied fibril formation of monomeric apo-SOD1 under non-agitated, near-physiological conditions, using the well-established pseudo-wildtype construct C6A/F50E/G51E/C111A, denoted pwt-SOD1 (Bertini *et al.*, 1994; Lindberg *et al.*, 2005; Teilum *et al.*, 2009), and the two variants $SOD1^{\Delta C}$ and $SOD1^{LL}$. The pwt-SOD1 construct renders the protein monomeric by introducing repulsive charges at the interface of the native dimer (F50E and G51E), and also obliterates potential disulfide bonds involving the two cysteines (C6 and C111) not involved in the native disulfide (C57–C146). $SOD1^{\Delta C}$ is a cysteine-free mutant that includes the C57S and C146S modifications in addition to those defining pwt-SOD1 (Khan *et al.*, 2017); it thus mimics the disulfide-reduced state of monomeric apo-SOD1, with the additional property that it cannot form intermolecular disulfide linkages. $SOD1^{LL}$ is a loop-less, 'naked' β-barrel variant, lacking the long loops IV and VII (Danielsson *et al.*, 2011), and is included here to address the role of the loops in fibril formation and for comparison with previous work on amyloid formation in mechanically agitated samples, which employed this variant (Lang *et al.*, 2012).

We used a combination of microplate fluorescence spectroscopy and transmission electron microscopy (TEM) to monitor fibril formation. We employed two types of microplates that differed in composition of the well surfaces, namely uncoated polystyrene (PS) plates and polyethylene glycol-coated polystyrene (PEG) plates. In addition, we added variable amounts of polystyrene nanoparticles to PEG sample wells. Polystyrene is a hydrophobic polymer known to interact with hydrophobic patches on solutes, such as those presented by unfolded proteins (Thormann *et al.*, 2008;

Faghihnejad and Zeng, 2012; Shen *et al.*, 2012; Lu *et al.*, 2016). By contrast, surfaces coated with polyethylene glycol present a non-ionic hydrophilic environment that mitigates protein adsorption and concomitant unfolding (Alcantar *et al.*, 2000; Shen *et al.*, 2012; Lu *et al.*, 2016).

In the fibril assay we used ThT fluorescence to detect fibril formation under experimental conditions that resemble the physiological environment in terms of the pH (7.0), temperature (37 °C), and absence of explicit mechanical agitation (i.e. without any stirring or shaking, except for the movements of the 96-well plate in the fluorescence instrument). We used monomeric protein freshly purified by analytical gel filtration, as described previously (Khan *et al.*, 2017); this treatment is vital to achieve reproducibility in fibril formation experiments involving SOD1, similar to previous observations for other amyloid-forming proteins (Hellstrand *et al.*, 2010; Grey *et al.*, 2011). As a result, the microplate fluorescence experiments usually resulted in satisfactory reproducibility with a relative variability in the onset of fibril formation of roughly 5–10%, but occasionally up to 30%; the lower numbers are on par with what has been observed for other cases, e.g. the Aβ peptide (Cukalevski *et al.*, 2015), which exhibits much shorter lag times. Due to the very long lag time, we did not follow the reaction to completeness, but simply monitored the onset of fibril build-up, which suffices as a proxy for the lag time in the present investigation where we aim for a qualitative interpretation. We verified that intrinsic ThT fluorescence does not degrade to any appreciable extent during the entire length of the experiments (Figure S1).

Disulfide reduction decreases the lag time for fibril formation in the presence of either hydrophilic or hydrophobic surfaces. We first investigated whether disulfide reduction is necessary to trigger fibril formation on hydrophobic PS plates, just as on PEG plates (Khan *et al.*, 2017). We find that disulfide reduction indeed appears to be a prerequisite for aggregation, at least on the time scale monitored here (up to 1 week), irrespective of the nature of the sample well surface, see Figure 2A, B; compare black lines depicting disulfide-oxidized SOD1 with green, blue and red lines, showing the effect of increasing degrees of disulfide reduction. Notably, the lag time is significantly shorter in experiments conducted using PS plates (Figure 2A), compared to the results obtained using PEG plates (Figure 2B), indicating that the hydrophobic surface catalyzes fibril nucleation. This observation is also born out for the $SOD1^{\Delta C}$ variant (Figures 2C, D), which mimics the fully disulfide-reduced state and consequently does not show any significant dependence on the TCEP concentration, as expected. Importantly, this result also demonstrates that TCEP does not interfere with fibril formation.

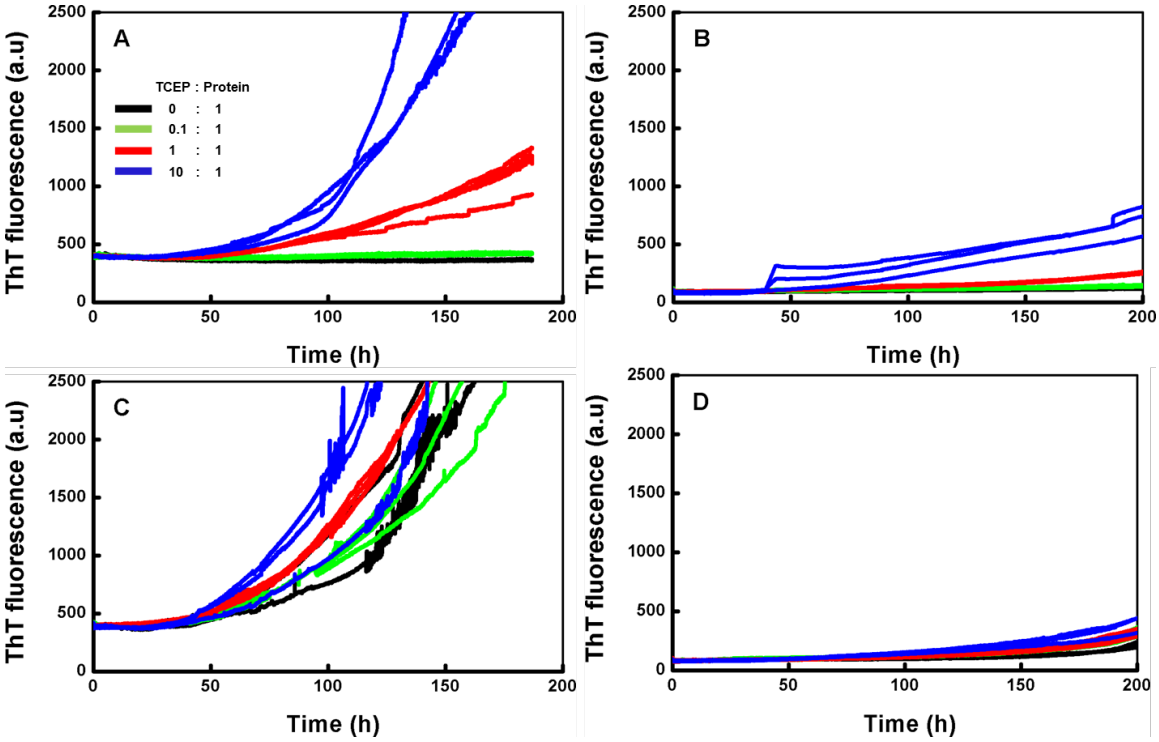

Figure 2. Comparison of lag time for fibril formation by SOD1 variants in hydrophobic polystyrene and hydrophilic PEGylated sample cells. Fibril formation experiments performed on (A, B) pwt-SOD1and (C, D) $SOD1^{\Delta C}$. ThT fluorescence was measured as a function of time with different concentrations of reducing agent (TCEP) added: blue, 10 equivalents of TCEP; red, 1 equivalent; green, 0.1 equivalent; black, no TCEP. Fibril formation experiments were performed using (A, C) hydrophobic PS plates and (B, D) hydrophilic PEG plates; the latter results are reproduced from our previous publication (Khan *et al.*, 2017). The SOD1 concentration was 200 μM and the temperature was 37 °C. The graphs include data from three replicate experiments. The discontinuity in the blue line of two replicates in panel B is likely caused by instrumental instabilities.

We carried out TEM experiments to verify that ThT fluorescence indeed results from fibril formation. Experiments conducted using PS plates show that reduced pwt-SOD1 and $SOD1^{\Delta C}$ give rise to fibrils with essentially identical morphology (Figure 3A,

B). These observations parallel our previous results obtained in PEG plates for the same SOD1 variants (Khan *et al.*, 2017). Thus, we conclude that SOD1$^{\Delta C}$ serves as a valid model for the disulfide-reduced wildtype protein in the context of either surface.

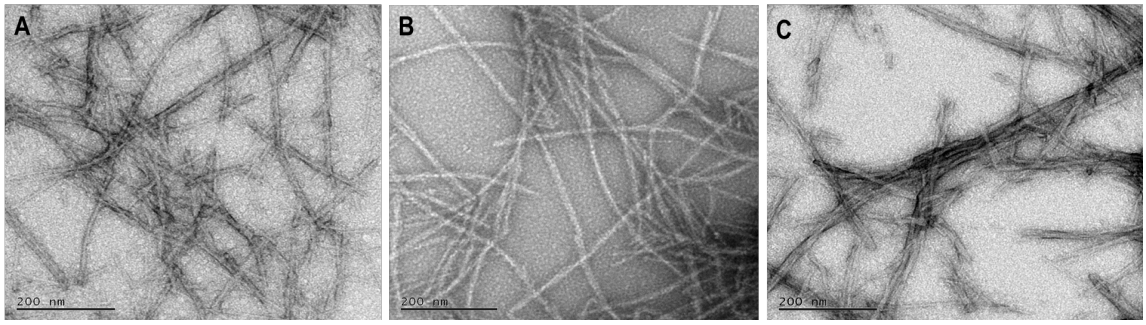

Figure 3. Transmission electron microscopy images of apo SOD1 amyloid fibrils formed in hydrophobic polystyrene plates. (A) Fibrils of pwt-SOD1 formed upon reduction of the native C57–C146 disulfide bond with TCEP. (B) Fibrils of the cysteine-free variant SOD1$^{\Delta C}$ formed without TCEP. (C) Fibrils of SOD1^{LL}formed in the presence of 2.74 M urea. The scale bar indicates 200 nm.

Urea promotes fibril formation in the presence of hydrophobic but not hydrophilic surfaces. We monitored the effect of increasing denaturant concentration on fibril formation by SOD1$^{\Delta C}$, disulfide-oxidized pwt-SOD1 and SOD1^{LL}, following published protocols (Khan *et al.*, 2017). In the case of SOD1$^{\Delta C}$, we varied the urea concentration in the ThT fluorescence assays to yield populations of the unfolded state of approximately $p_U < 5\%$, $p_U \approx 50\%$, or $p_U > 99\%$. Increasing the population of unfolded SOD1$^{\Delta C}$ to $p_U \approx$ 50% (Figure 4A, red curve) leads to decreased lag time on PS plates. However, at the highest denaturant concentration, where $p_U > 99\%$ (Figure 4A, blue curve), no fibrils are

detected within the time frame of the experiment (approximately 1 week). Aggregates apparently become destabilized at the highest urea concentration, thereby preventing fibril formation, as observed previously (Lang *et al.*, 2012). The decreased lag time resulting from addition of lower amounts of urea might be expected since unfolding leads to exposure of hydrophobic regions of the protein, which are known to favour aggregation on hydrophobic surfaces, and is consistent with results reported in studies where shaking or shirring with teflon beads were employed (Chattopadhyay and Valentine, 2009). In contrast, we previously observed that denaturant does not induce fibril formation on PEG plates under otherwise identical experimental conditions, see Figure4B (Khan *et al.*, 2017). It thus appears that aggregates become relatively less destabilized by denaturants when formed on hydrophobic surfaces, resulting in more efficient fibril formation. Thus, the nature of the extraneous surface available to the protein modulates the aggregation propensity of the protein and its response to denaturant.

Experiments using disulfide oxidized pwt-SOD1 show that the intact disulfide bridge prevents aggregation of the unfolded form on both PS and PEG plates under the same conditions as those reported above for $SOD1^{\Delta C}$ (Figure 4C, D). Similar to disulfide-reduced SOD1, the disulfide-oxidized form is expected to expose hydrophobic patches upon unfolding, but this feature is apparently not sufficient for fibril nucleation to take place.

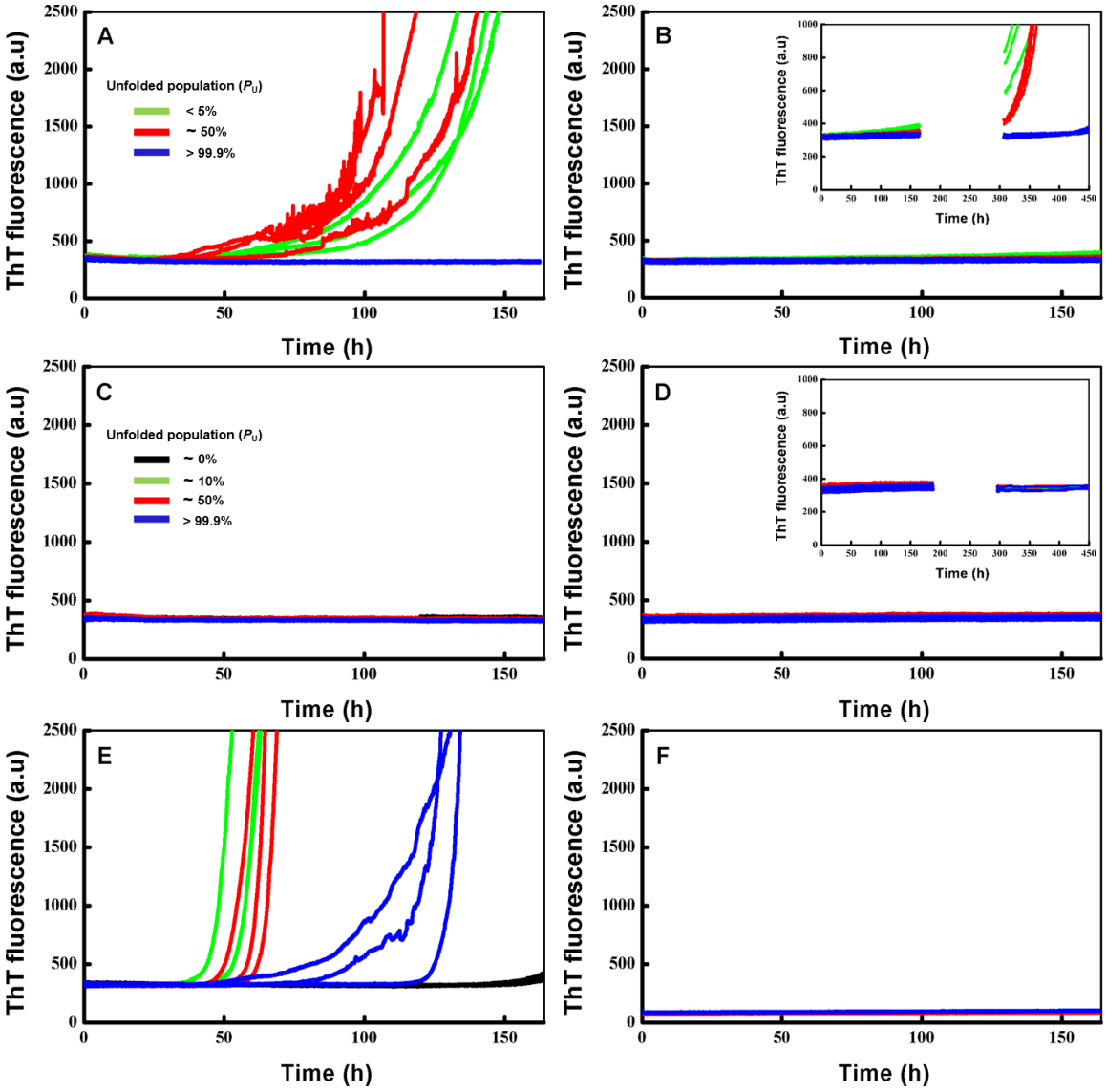

Figure 4. Fibril formation in hydrophobic polystyrene and hydrophilic PEGylated plates shows opposite responses to unfolding by urea. Fibril formation experiments with varying concentrations of urea yielding different populations of the unfolded state: (A, B) $SOD1^{\Delta C}$: p_U < 5% (green), no urea added; $p_U \approx 50\%$ (red), 0.22 ± 0.01 M urea; and p_U > 99% (blue), 2.58 ± 0.03 M urea. (C, D) disulfide-oxidized pwt-SOD1: $p_U \approx 0\%$ (black), no urea added; $p_U \approx 10\%$ (green), 1.19 ± 0.01 M urea; and $p_U \approx 50\%$ (red), 1.81 ± 0.03 M urea; and p_U > 99% (blue), 3.75 ± 0.05 M urea. (E, F) $SOD1^{LL}$: $p_U = 0\%$ (black), no urea added; $p_U \approx 10\%$ (green), 1.82 ± 0.01 M urea added; $p_U \approx 50\%$ (red), 2.74 ± 0.02 M urea; and p_U > 99% (blue), 5.70 ± 0.05

M urea. Fibril formation experiments were performed using (A, C, E) hydrophobic PS plates and (B, D, F) hydrophilic PEG plates; the latter results are reproduced from our previous publication (Khan *et al.*, 2017). Insets in panels B and D show results for an extended time range up to 450 h. The SOD1 concentration was 200 μM and the temperature was 37 °C. The graphs include data from three replicate experiments.

Next, we repeated the same experiments on the previously studied variant $SOD1^{LL}$, in which the long loops IV (residues 49–81) and VII (124–139) have been replaced by Gly-Ala-Gly tripeptide linkers and C146 has been replaced by Ser so as to prevent intermolecular disulfide bonds from forming (Lang *et al.*, 2012). We compared the aggregation behavior of $SOD1^{LL}$ with those of $SOD1^{\Delta C}$ and disulfide-linked pwt-SOD1, using both PS and PEG plates. In experiments conducted using PS plates, $SOD1^{LL}$ forms fibrils at all urea concentrations (Figure 4E). We also visualized $SOD1^{LL}$ amyloid fibrils using TEM (Figure 3C) and found them to be highly similar to those formed by disulfide-reduced pwt-SOD1 and $SOD1^{\Delta C}$ (cf. Figures 3A and B). The lag-time was longer at the highest urea concentration ($p_U \sim 99\%$), compared to the lag-time at lower urea concentrations, which is in agreement with the results obtained for $SOD1^{\Delta C}$ (Figure 4A), but different from disulfide-oxidized pwt-SOD1, which did not form fibrils at any urea concentration (Figure 4C). By contrast, $SOD1^{LL}$ resists aggregation in experiments conducted using PEG plates, (Figure 4F), similar to what is observed for pwt-SOD1 in the disulfide-oxidized state, but different from the less stable variants disulfide-reduced pwt-SOD1and $SOD1^{\Delta C}$ (Khan *et al.*, 2017).

The observed differences in fibril formation behaviour of the different SOD1 variants in PS plates can be explained in part by differences in stability towards unfolding. The stabilities of disulfide-reduced pwt-SOD1, $SOD1^{\Delta C}$, disulfide-linked pwt-SOD1 and $SOD1^{LL}$ increase in the order listed here. The higher urea concentrations required to generate a given population of the unfolded state for the more stable variants are also expected to destabilize aggregates and fibrils to a greater extent than that achieved by the lower denaturant concentrations used in experiments on disulfide-reduced pwt-SOD1 and $SOD1^{\Delta C}$. Thus, we might expect disulfide-oxidized pwt-SOD1 to be more resistant than disulfide-reduced pwt-SOD1 and $SOD1^{\Delta C}$ towards urea-induced aggregation in PS plates. However, $SOD1^{LL}$ does form fibrils on PS plates (Figure 4E) even though this variant is more stable than disulfide-linked pwt-SOD1, which does not form fibrils on either PS or PEG plates (Figures 4C, D). This apparent inconsistency might be explained by differences in net electrostatic charge of the variants: $SOD1^{LL}$ is less charged (estimated to –2 at pH 7) than the other variants (–5 at pH 7), which implies that aggregation of $SOD1^{LL}$ is less impeded by electrostatic repulsion between monomers. Alternatively, the different behaviors might be related to the presence of the native disulfide bond in disulfide-oxidized pwt-SOD1, but not in the other variants, suggesting that cleavage of the disulfide bond is required for fibril formation irrespective of whether SOD1 is predominantly folded or unfolded. In either case, the results summarized in Figure 4 are consistent with a model where unfolded SOD1 nucleates on extraneous hydrophobic surfaces to form fibrils.

Taken together, our results and previously published data (Lang *et al.*, 2012) suggest that hydrophobic surfaces catalyze fibril nucleation and that unfolding of the protein further speeds up this process, most likely by increasing the exposure of hydrophobic patches on the protein and thereby enhancing adsorption to the surfaces. Apparently, the adsorption of the protein onto the hydrophobic surface overrides the destabilization of protein aggregates by denaturants in solution, so that fibril nucleation occurs more efficiently in the presence of denaturant.

Increasing the hydrophobic surface area in the sample well accelerates fibril formation of unfolded SOD1. Above we have shown that disulfide-reduced pwt-SOD1, $SOD1^{\Delta C}$ and $SOD1^{LL}$ all display enhanced fibril formation in PS plates, which further increases upon unfolding of the protein. To firmly establish that this phenomenon is due to surface catalyzed nucleation on the hydrophobic surface, we carried out fibril formation experiments with unfolded $SOD1^{LL}$ on PEG plates in the presence of polystyrene nanoparticles, which are intrinsically hydrophobic in nature.

Addition of PS nanoparticles in a concentration that generates a surface area matching that estimated for the sample well of a PS plate leads to efficient nucleation of fibrils (Figure 5A), in sharp contrast to results in PEG plates without PS nanoparticles (Figure 4F). A comparison with the results obtained in PS plates (Figure 4E) indicates that the nanoparticles are more efficient in catalyzing nucleation at all urea concentrations than is the surface of the well in the PS plate, probably because the nanoparticles are spread throughout the sample volume and hence are more accessible to the protein. As a control, we also performed experiments with nanoparticles, but without

any protein, to verify that nanoparticles do not influence ThT fluorescence in a time-dependent manner. Addition of nanoparticles leads to light scattering, which manifests itself as an offset in the signal intensity that increases with increasing nanoparticle concentration (see Figure S2).

Next we performed a series of experiments with increasing hydrophobic surface area, generated by increasing the amount of PS nanoparticles, for each of the four different concentrations of urea (0 M, 1.82 M, 2.74 M and 5.7 M; corresponding to $p_U \approx$ 0%, 10%, 50% and $p_U >$ 99%). We increased the hydrophobic surface area to 5 or 10 times that available in a PS sample well. As shown in Figures 5B–D, the lag time decreases progressively with increasing hydrophobic surface area whenever $SOD1^{LL}$ is destabilized by the addition of urea, whereas folded $SOD1^{LL}$ (no urea added) does not form fibrils even at the highest hydrophobic surface area (Figure 5E). Thus, we conclude that unfolding appears to be a prerequisite for surface dependent SOD1 aggregation.

We note that nanoparticles apparently lead to a change in the response of SOD1 fibril formation towards urea, compare Figures 5A and 4E. In the presence of nanoparticles, fibril formation appears to occur with a shorter lag-time but slower rate at the highest urea concentration ($p_U \sim$ 99%) than it does at the lower urea concentrations ($p_U \sim$ 10–50%), compare Figure 5D with Figures 5B and 5C. A complex interdependence between the amount of nanoparticle surface area and solvent conditions can be expected (Linse *et al.*, 2007), which is also reflected by Figure 5. However, at present we cannot interpret this interesting result, which calls for future investigations.

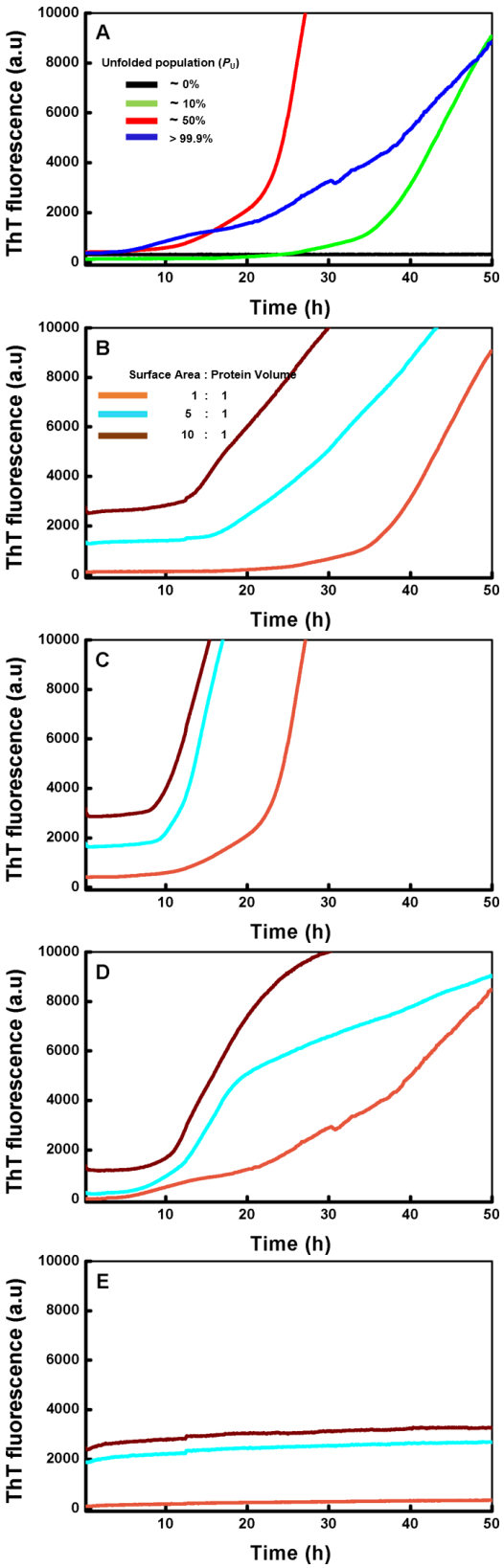
A
Unfolded population (P_U)
~ 0%
~ 10%
~ 50%
> 99.9%
B
Surface Area : Protein Volume
1 : 1
5 : 1
10 : 1
C
D
E
ThT fluorescence (a.u)
Time (h)
0
2000
4000
6000
8000
10000
10
20
30
40
50

Figure 5. Fibril formation of $SOD1^{LL}$ in hydrophilic PEGylated plate with added polystyrene nanoparticles. Fibril formation experiments on $SOD1^{LL}$ with (A) varying concentrations of urea, yielding populations of the unfolded state of: p_U = 0% (black), without urea, $p_U \approx$ 10% (green), 1.82 ± 0.01 M urea added; $p_U \approx$ 50% (red), 2.74 ± 0.02 M urea; and $p_U >$ 99% (blue), 5.70 ± 0.05 M urea. The amount of PS nanoparticles was calculated to match the surface area of a sample well. (B, C) Different concentrations of PS nanoparticles added to PEG sample wells: orange, 1 equivalent of PS nanoparticle surface area corresponding to that of a sample well; cyan, 5 equivalents; brown, 10 equivalents. Fibril formation experiments were initiated with (B) $p_U \approx$ 10%, 1.82 ± 0.01 M urea added; (C) $p_U \approx$ 50%, 2.74 ± 0.02 M urea; and (D) $p_U >$ 99%, 5.70 ± 0.05 M urea. (E) p_U = 0%, no urea added. The higher signal intensity observed at higher concentrations of nanoparticles is due to light scattering by the nanoparticles (Figure S2). The SOD1 concentration was 200 μM and the temperature was 37 °C.

Concluding remarks. Using a well-defined in vitro model system, we have investigated how the nature and area of surrounding surfaces affect fibril formation by SOD1. We found that hydrophobic polystyrene surfaces promote fibril formation and that unfolding of SOD1 by addition of denaturant further decreases the lag time for fibril formation in this case. This result indicates that unfolded SOD1 adsorbs to hydrophobic surfaces, which then catalyze fibril nucleation. Increasing the available surface area by addition of polystyrene nanoparticles proportionally decreases the lag time, further bolstering this conclusion. These results are in sharp contrast to our previous results obtained using hydrophilic, non-binding PEG-ylated microplates, where the addition of denaturant results in the opposite behavior, i.e. an increase in lag time for fibril formation. Taken together, our results strongly suggest that the mechanistic details of SOD1 fibril formation depend sensitively on the experimental conditions in vitro and that surface-

catalyzed and in-solution nucleation might involve different conformational states of SOD1. The results further suggest that different pathways for SOD1 amyloid formation might prevail in vivo, given the complex cell environment that includes a variety of surfaces and co-solutes with different chemical composition.

ASSOCIATED CONTENT

Supporting Information

ThT fluorescence microplate control experiments of ThT fluorescence over time in pure buffer (without SOD1 or nanoparticles); ThT fluorescence microplate control experiments of ThT fluorescence over time in buffer with nanoparticles but without SOD1; MS spectra of $SOD1^{LL}$; analytical gel filtration chromatogram; Tables summarizing experimental conditions and results (PDF).

AUTHOR INFORMATION

Corresponding author

e-mail: mikael.akke@bpc.lu.se

Acknowledgments

We thank Kristine Steen Jensen, Risto Cukalevski and Sara Linse for helpful discussions and SL for kindly providing access to microplate fluorescence instruments. This work was supported by The Swedish Research Council (621-2014-5815 to MA) and the Göran Gustafsson Foundation for Research in Natural Sciences and Medicine (MA). MAIK was

supported by the European Commission via the Erasmus Mundus Europe Asia scholarship program and by the Carl Trygger Foundation.

REFERENCES

Abdolvahabi,A., Shi,Y., Rasouli,S., Croom,C.M., Chuprin,A. and Shaw,B.F. (2017) *Biophys. J.*, **112**, 250–264.

Aisenbrey,C., Borowik,T., Byström,R., Bokvist,M., Lindström,F., Misiak,H., Sani,M.A. and Gröbner,G. (2008) *Eur. Biophys. J.*, **37**, 247–255.

Ajroud-Driss,S. and Siddique,T. (2015) *BBA - Mol Basis Dis*, **1852**, 679–684.

Alcantar,N.A., Aydil,E.S. and Israelachvili,J.N. (2000) *J. Biomed. Mater. Res.*, **51**, 343–351.

Banci,L., Barbieri,L., Bertini,I., Luchinat,E., Secci,E., Zhao,Y. and Aricescu,A.R. (2013) *Nat. Chem. Biol.*, **9**, 297–299.

Bertini,I., Piccioli,M., Viezzoli,M.S., Chiu,C.Y. and Mullenbach,G.T. (1994) *Eur. Biophys. J.*, **23**, 167–176.

Bosco,D.A., Morfini,G., Karabacak,N.M., *et al.* (2010) *Nat. Neurosci.*, **13**, 1396-U133.

Chattopadhyay,M., Durazo,A., Sohn,S.H., Strong,C.D., Gralla,E.B., Whitelegge,J.P. and Valentine,J.S. (2008) *Proc. Natl. Acad. Sci. U. S. A.*, **105**, 18663–18668.

Chattopadhyay,M., Nwadibia,E., Strong,C.D., Gralla,E.B., Valentine,J.S. and Whitelegge,J.P. (2015) *J. Biol. Chem.*, **290**, 30624–30636.

Chattopadhyay,M. and Valentine,J.S. (2009) *Antioxid. Redox Signal.*, **11**, 1603–1607.

Chiti,F. and Dobson,C.M. (2006) *Annu. Rev. Biochem.*, **75**, 333–366.

Chiti,F. and Dobson,C.M. (2009) *Nat. Chem. Biol.*, **5**, 15–22.

Cukalevski,R., Yang,X., Meisl,G., Weininger,U., Bernfur,K., Frohm,B., Knowles,T.P.J. and Linse,S. (2015) *Chem. Sci.*, **6**, 4215–4233.

Danielsson,J., Kurnik,M., Lang,L. and Oliveberg,M. (2011) *J. Biol. Chem.*, **286**, 33070–33083.

Dobson,C.M. (2003) *Nature*, **426**, 884–890.

Faghihnejad,A. and Zeng,H. (2012) *Soft Matter*, **8**, 2746–2759.

Forsberg,K., Jonsson,P.A., Andersen,P.M., *et al.* (2010) *PLoS One*, **5**.

Grey,M., Linse,S., Nilsson,H., Brundin,P. and Sparr,E. (2011) *J. Parkinsons. Dis.*, **1**, 359–371.

Gruzman,A., Wood,W.L., Alpert,E., *et al.* (2007) *Proc. Natl. Acad. Sci. U. S. A.*, **104**, 12524–12529.

Hellstrand,E., Boland,B., Walsh,D.M. and Linse,S. (2010) *ACS Chem. Neurosci.*, **1**, 13–18.

Hörnberg,A., Logan,D.T., Marklund,S.L. and Oliveberg,M. (2007) *J. Mol. Biol.*, **365**, 333–342.

Hough,M.A., Grossmann,J.G., Antonyuk,S. V, *et al.* (2004) *Proc. Natl. Acad. Sci. U. S. A.*, **101**,

5976–5981.
Karch,C.M. and Borchelt,D.R. (2008) *J. Biol. Chem.*, **283**, 13528–13537.
Karch,C.M., Prudencio,M., Winkler,D.D., Hart,P.J. and Borchelt,D.R. (2009) *Proc. Natl. Acad. Sci. U. S. A.*, **106**, 7774–7779.
Khan,M.A.I., Respondek,M., Kjellström,S., Deep,S., Linse,S. and Akke,M. (2017) *ACS Chem. Neurosci.*
Khare,S.D., Caplow,M. and Dokholyan,N. V (2004) *Proc. Natl. Acad. Sci. U. S. A.*, **101**, 15094–15099.
Knowles,T.P.J., Waudby,C.A., Devlin,G.L., Cohen,S.I.A., Welland,M.E. and Dobson,C.M. (2009) *Science (80-.).*, **326**, 1533–1537.
Lang,L.S., Kurnik,M., Danielsson,J. and Oliveberg,M. (2012) *Proc. Natl. Acad. Sci. U. S. A.*, **109**, 17868–17873.
Leinartaitè,L., Saraboji,K., Nordlund,A., Logan,D.T. and Oliveberg,M. (2010) *J. Am. Chem. Soc.*, **132**, 13495–13504.
Lindberg,M.J., Byström,R., Boknäs,N., Andersen,P.M. and Oliveberg,M. (2005) *Proc. Natl. Acad. Sci. U. S. A.*, **102**, 9754–9759.
Lindberg,M.J., Tibell,L. and Oliveberg,M. (2002) *Proc. Natl. Acad. Sci. U. S. A.*, **99**, 16607–16612.
Linse,S., Cabaleiro-Lago,C., Xue,W.F., Lynch,I., Lindman,S., Thulin,E., Radford,S.E. and Dawson,K.A. (2007) *Proc. Natl. Acad. Sci.*, **104**, 8691–8696.
Lu,Q., Tang,Q., Xiong,Y., Qing,G. and Sun,T. (2016) *Materials (Basel).*, **9**, 740;doi10.3390/ma9090740.
Luchinat,E., Barbieri,L., Rubino,J.T., Kozyreva,T., Cantini,F. and Banci,L. (2014) *Nat. Commun.*, **5**, 5502.
Luheshi,L.M., Crowther,D.C. and Dobson,C.M. (2008) *Curr. Opin. Chem. Biol.*, **12**, 25–31.
Moores,B., Drolle,E., Attwood,S.J., Simons,J. and Leonenko,Z. (2011) *PLoS One*, **6**, e25954.
Morgan,S. and Orrell,R.W. (2016) *Brit Med Bull*, **119**, 87–97.
Morinaga,A., Hasegawa,K., Nomura,R., Ookoshi,T., Ozawa,D., Goto,Y., Yamada,M. and Naiki,H. (2010) *Biochim. Biophys. Acta-Proteins Proteomics*, **1804**, 986–995.
Oztug Durer,Z.A., Cohlberg,J.A., Dinh,P., *et al.* (2009) *PLoS One*, **4**.
Pronchik,J., He,X., Giurleo,J.T. and Talaga,D.S. (2010) *J. Am. Chem. Soc.*, **132**, 9797–9803.
Rakhit,R., Crow,J.P., Lepock,J.R., Kondejewski,L.H., Cashman,N.R. and Chakrabartty,A. (2004)

J. Biol. Chem., **279**, 15499–15504.
Roberts,B.L.T., Patel,K., Brown,H.H. and Borchelt,D.R. (2012) *PLoS One*, **7**, e47838.
Sekhar,A., Rumfeldt,J.A.O., Broom,H.R., Doyle,C.M., Bouvignies,G., Meiering,E.M. and Kay,L.E. (2015) *Elife*, **4**, e07296.
Shen,L., Adachi,T., Bout,D. Vanden and Zhu,X.Y. (2012) *J. Am. Chem. Soc.*, **134**, 14172–14178.
Stefani,M. (2007) *Neuroscientist*, **13**, 519–531.
Tainer,J.A., Getzoff,E.D., Beem,K.M., Richardson,J.S. and Richardson,D.C. (1982) *J. Mol. Biol.*, **160**, 181–217.
Teilum,K., Smith,M.H., Schulz,E., Christensen,L.C., Solomentsev,G., Oliveberg,M. and Akke,M. (2009) *Proc. Natl. Acad. Sci. U. S. A.*, **106**, 18273–18278.
Thormann,E., Simonsen,A.C., Hansen,P.L. and Mouritsen,O.G. (2008) *Langmuir*, **24**, 7278–7284.
Valentine,J.S., Doucette,P.A. and Potter,S.Z. (2005) *Annu. Rev. Biochem.*, **74**, 563–593.
Wang,J., Xu,G.L. and Borchelt,D.R. (2006) *J. Neurochem.*, **96**, 1277–1288.
Wang,J., Xu,G.L., Gonzales,V., Coonfield,M., Fromholt,D., Copeland,N.G., Jenkins,N.A. and Borchelt,D.R. (2002) *Neurobiol. Dis.*, **10**, 128–138.
Xue,W.F., Homans,S.W. and Radford,S.E. (2008) *Proc. Natl. Acad. Sci.*, **105**, 8926–8931.
Zhu,M., Souillac,P.O., Ionescu-Zanetti,C., Carter,S.A. and Fink,A.L. (2002) *J. Biol. Chem.*, **277**, 50914–50922.

Editor: Valerie Daggett